Environmental Modelling and Software 119 (2019) 99–110

Contents lists available at ScienceDirect

Environmental Modelling & Software

journal homepage: www.elsevier.com/locate/envsoft

Merging radar and gauge information within a dynamical model combination framework for precipitation estimation in cold climates

Kuganesan Sivasubramaniam[a,*], Ashish Sharma[b], Knut Alfredsen[a]

[a] Department of Civil and Environmental Engineering, Norwegian University of Science and Technology, 7491, Trondheim, Norway
[b] School of Civil and Environmental Engineering, University of New South Wales, Sydney, NSW, 2052, Australia

ARTICLE INFO

Keywords:
Merging radar and gauge precipitation
Dynamic model combination
Nonparametric radar precipitation
K-nearest neighbour
Spatial precipitation and temperature
Cold climate precipitation

ABSTRACT

This study presents a dynamic forecast combination approach adapted to incorporate multiple sources of precipitation. Dynamic combination serves to utilise the varying merit each data source exhibits with time. The dynamic model combination framework presented merges a nonparametric k-nearest neighbour (k-nn) estimation of radar precipitation with Thin Plate Spline (TPS) interpolated gauge precipitation. Since air temperature is an essential variable to discriminate the phase of the precipitation in cold climates, this study uses radar precipitation and air temperature as the two variables in the dynamic combination algorithm. The merging of k-nn and TPS estimates is shown to reduce the RMSE by 25% compared to the original radar precipitation rates. The usefulness of air temperature is found not to be as significant in the combination as it is in the formulation of the nonparametric radar precipitation fields for cold incident temperatures.

1. Introduction

Continuous simulations of streamflow and catchment water storage using distributed hydrological models require accurate precipitation input at high spatial resolution (Syed et al., 2003; Smith et al., 2004; Beven, 2012). It is often shown that existing precipitation networks in many places are not dense enough to capture the spatial variation of precipitation events (Kirchner, 2009; Hwang et al., 2012). Precipitation measurement by remote sensing has a great potential to fulfill the need for distributed input data measured at a catchment scale (Krajewski and Smith, 2002; Woldemeskel et al., 2013). Presently, weather radars provide precipitation estimates with high spatial (at a standard resolution of 1 km × 1 km) and temporal (hourly and sub-hourly) resolution. However, weather radar measures precipitation indirectly using remote sensing techniques and measurements are subject to several sources of errors and uncertainties (Chumchean et al., 2006b; Villarini and Krajewski, 2010; Berne and Krajewski, 2013; Abdella, 2016).

Weather radar transmits electromagnetic waves and measures the energy backscattered by the hydrometeors in the atmosphere as reflectivity. The reflectivity is then converted to ground precipitation rates. Typically, parametric power law relationship often called as Z - R equation ($Z = aR^b$) is used in the conversion of radar reflectivity (Z) to ground precipitation rates (R). The constant values of a = 200 and b = 1.6 derived by Marshall and Palmer (1948) for rain are generally used regardless of climate region. However, these parameters are not constant (Wilson and Brandes, 1979) and they are related to drop size distribution of hydrometeors in the atmosphere. Drop size distribution varies with the type and phase of the precipitation (Joss et al., 1990; Uijlenhoet, 2001; Chumchean et al., 2008). Due to errors and uncertainties in the measurement of reflectivity as well as in the conversion of reflectivity to ground precipitation, advances and advantages of radar precipitation data are not fully used in widespread hydrological applications so far (Chumchean et al., 2003; Berne and Krajewski, 2013).

To model radar rainfall uncertainty, Ciach et al. (2007) used the nonparametric kernel regression method. Such nonparametric approaches can be more effective than parametric alternatives as fewer assumptions about the processes being modelled needs invoking while sufficient observational data exist (Silverman, 1986; Mehrotra and Sharma, 2006). While ability to adapt to the data locally is a strength of the nonparametric approaches, they can result in local biases due to outliers. Villarini et al. (2008) compared their nonparametric approach with a copula based method and found that the performance was as equal or higher than copula. Hasan et al. (2016b) presented a kernel based nonparametric method to improve radar rainfall estimates using the conditional probability distribution of past observed reflectivity and gauged rainfall. Sivasubramaniam et al. (2018) extended the Hasan

* Corresponding author.
E-mail addresses: kuganesan.sivasubramaniam@ntnu.no (K. Sivasubramaniam), A.Sharma@unsw.edu.au (A. Sharma), knut.alfredsen@ntnu.no (K. Alfredsen).

https://doi.org/10.1016/j.envsoft.2019.05.013
Received 27 November 2018; Received in revised form 15 May 2019; Accepted 17 May 2019
Available online 27 May 2019

et al. (2016b) univariate nonparametric approach of radar precipitation estimates to bivariate with the use of near surface air temperature as a covariate to improve the radar precipitation estimates in cold climates.

Accurate estimates of precipitation data are required for engineering design and management in small basins, particularly with the intense local rainfall events where the hydrological processes impelled by rainfall rates play a relatively higher role than the hydraulic processes of flood wave propagation (Krajewski and Smith, 2002). Weather radar with its extended spatial coverage can monitor many small catchments that otherwise remain ungauged without any precipitation observations (Berne and Krajewski, 2013). Moreover, as precipitation is an intermittent variable and various difficulties in measuring precipitation precisely, accurate estimation of spatial distribution of precipitation in the river basin using sparse gauge network alone is a challenging task (Hwang et al., 2012). As a result, distributed and physically based hydrological models are often limited by the accurate spatial variability of precipitation input data (Syed et al., 2003).

To obtain the spatial distribution of precipitation in a catchment from available gauges which are often unevenly distributed, spatial interpolation techniques are required. A range of spatial interpolation techniques are available in the literature, from simple methods (e.g. arithmetic mean, nearest neighbour, Thiessen polygon and inverse distance weighting) to advanced and more complex approaches (e.g. multiple linear regression, thin plate smoothing splines, kriging, genetic algorithms, conditional bias penalized kriging and Copula). A review of different interpolation methods is presented by Hwang et al. (2012) where the gauge is a single sensor of precipitation. Even with the use of advanced spatial interpolation techniques, it is a challenging task to get a distributed precipitation field in a sparsely gauged area.

It is often shown that compared to gauges, radars capture the spatial variation of precipitation relatively well despite errors in their quantitative information. Several studies (Chumchean et al., 2006a; Haberlandt, 2007; Goudenhoofdt and Delobbe, 2009) have shown that merging of radar precipitation estimates with gauge precipitation can improve precipitation estimates. The merging approach is as old as the arrival of weather radar data for hydrological applications. The focus of earlier studies has been to correct the bias in the radar precipitation estimation using gauge observations. Mean Field Bias (MFB) correction is a simple bias correction method that is broadly used. The MFB method assumes a uniform multiplicative error in the radar estimates and it estimates the ratio of the accumulated radar precipitation and accumulated gauge precipitation from a number of radar-gauge pairs as a multiplicative adjustment factor. Brandes (1975) proposed a correction factor at each gauge location with subsequent interpolation over the radar field. Chumchean et al. (2006a) applied Kalman filter to improve the MFB estimates.

Subsequent focus on merging radar and gauge data has utilised the spatial variability of the radar to further improve the spatial interpolation of gauges. Several merging methods with the use of geostatistical techniques with different degree of complexity have been proposed. Some of the geostatistical merging methods in literature are cokriging (Krajewski, 1987), kriging with external drift (KED) (Berndt et al., 2014), conditional merging (Sinclair and Pegram, 2005) and copula-based assimilation (Vogl et al., 2012). The geostatistical methods generally consider gauge as a primary source and radar as secondary source for the merging (Goudenhoofdt and Delobbe, 2009); however, Rabiei and Haberlandt (2015) showed that quality of the quantitative radar data is still important factor in conditional merging.

Hasan et al. (2016a,b), argue that if errors associated with the precipitation field derived from radar and gauge can be quantified correctly, the two data sources can be merged without abandoning the quantitative information from the radar. This approach can be promising in sparsely gauged regions because intensity information from radar is to be extracted by extending the error structure identified from gauged regions to ungauged regions. Combination of two sources of information using error variance has its basis in economic forecast combination (Bates and Granger, 1969). When two set of forecasts are combined, the resulting forecast can have lower mean square error than both original forecasts (Bates and Granger, 1969). The forecast combination approach has been applied in hydrometeorology (Wasko et al., 2013) along with other areas.

The forecast combination methodology is prevalent in combining seasonal forecasts from multiple climate models. These studies have reported the usefulness of dynamic weighting in combination instead of simple static combination (Chowdhury and Sharma, 2009, 2011; Devineni and Sankarasubramanian, 2010; Khan et al., 2014; Kim et al., 2016). In the dynamic combination, the combination weights change over time to capture temporal variation locally. Hasan et al. (2016a) evaluated different combination approaches in the context of merging radar and gauge rainfall data. They found that covariance-based methods gave better results compared to non-covariance based methods and showed the usefulness of dynamic approach. Hasan et al. (2016b) presented a covariance based dynamic model combination framework to combine radar and gauge rainfall data sources. In their study, a kernel based nonparametric approach was used to estimate rainfall estimates and then nonparametric radar rainfall estimates were merged with copula based spatially interpolated rainfall field for a tropical climate. In the dynamic model combination, similar events were identified using a k-nearest neighbour approach with reflectivity as a single variable to estimate the error covariance matrix and weights.

In cold climates, precipitation occurs with different phases (snow, rain or a mixture of snow and rain) and similar events can be specified not only based on the intensity information but also the phase of the precipitation. Several studies have shown that air temperature is intrinsic to the phase of the precipitation (Auer Jr, 1974; Killingtveit, 1976; Rohrer, 1989; Fassnacht et al., 2001). Air temperature is an essential variable to differentiate two similar events with different phase (snow or rain), but the same intensity (Al-Sakka et al., 2013). Fassnacht et al. (1999, 2001) used the near surface air temperature observations to adjust the radar precipitation estimation. Sivasubramaniam et al. (2018) showed that the use of air temperature as a second covariate in the k-nearest neighbour (k-nn) nonparametric model reduces the root mean squared error significantly and improves the radar precipitation estimates in colder temperatures. As similar to the Sivasubramaniam et al. (2018) approach, air temperature can also be used as an additional variable to identify similar events within the dynamic model combination framework to further improve the combination estimates in cold climates.

The overall objective of this study is to improve the precipitation estimates with high spatiotemporal resolution. The primary focus is to merge radar precipitation field with existing gauge observations to generate improved continuous hourly precipitation field for the region. For that, first, we adjust the hourly radar precipitation rates using the k-nearest neighbour nonparametric method and then we use the dynamic model combination framework to merge the nonparametric estimates with spatially interpolated precipitation gauge data using thin plate spline (TPS) interpolation. We evaluate whether the use of air temperature as an additional variable can be useful for dynamic model combination as is found for the nonparametric estimation.

2. Material and methods

2.1. Study area

The study area for the current research is 100 km radius from Hurum radar station in Norway (an area of about 31000 km^2) as shown in Fig. 1. The Hurum radar station is located at 59.63° N latitude and 10.56° E longitude and it is about 30 km from the Norwegian capital city, Oslo. It is a C band installation with a wavelength of 5.319 cm and a coverage radius of approximately 240 km. The Hurum radar has been in operation since November 2010 and monitors the southeastern part of Norway and part of Sweden; the coverage area consists of six

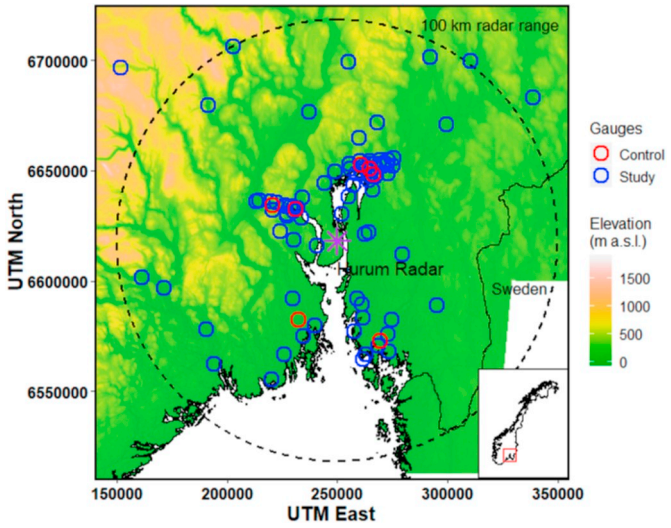

Fig. 1. The Hurum radar station (purple star mark) and its coverage of radius 100 km (black stippled line) and precipitation gauge locations overlaid on the topography of the study area, Oslo region of Norway. The gauges used in the computation (blue circles) and left for verification (red circles). (For interpretation of the references to colour in this figure legend, the reader is referred to the Web version of this article.)

Norwegian counties where nearly 40% of the population live.

Within the study area, 94 precipitation gauges are in operation with available hourly precipitation data for the study. The precipitation gauges are tipping bucket gauges (most of them are Lambrecht and Nivus RM-202 brands) and weighing gauges (Geonor brand) with an "Alter" windshield. Fig. 1 shows the precipitation gauge locations overlaid on the topography of the study area. Seven-gauges were left from the computations in order to verify the approach at ungauged pixels. In Fig. 1, the 87 gauges which were used in the computation are displayed with blue circles and the 7 gauges with red. Looking at Fig. 1, precipitation gauges are not evenly distributed. A relatively dense network of gauges exists near urban areas along the coast and a sparse network of gauges exist in the rest of the area. Further, it can be seen that the inland mountainous areas remain mostly ungauged without precipitation gauges with hourly measurements.

Mean annual precipitation in the study area is between 1000 and 1500 mm based on the climatology for the period 1961 to 2017 (http://www.senorge.no/). The precipitation in the study region can broadly be divided into three categories: frontal, orographic and convective precipitation. The convective precipitation is most dominant during the warmer summer months. The annual mean temperature is in the range of 2° - 10° C in the study region. The January mean is near freezing at the coast and down to −10° - −15° C inland. The maximum summer temperature is mostly in the 20° - 25° C range.

2.2. Data

At present, the Norwegian Meteorological Institute (met.no) operates nine C-band Doppler weather radar installations including the Hurum radar station. The Norwegian radar network covers the entire land surface of Norway and they scan the atmosphere with a 7.5 min temporal resolution, with this resolution being 15 min until June 2013. The raw radar volume scan from the radar stations are processed and quality controlled by met.no, and then met.no generates and distributes various radar products to end users (Elo, 2012). One of the products from met.no is Surface Rainfall Intensity (SRI). The mosaics of nine radars' SRI data covering entire Norway are available for the public to use in practical applications.

The quality of the measured reflectivity can vary from pixel to pixel due to the nature of remote sensing measurements. Topography and distance from the radar station affect the radar measurement of precipitation and introduce errors; these include anomalous propagation, ground clutter, beam blocking and attenuation (Germann and Joss, 2004). In a mountainous region like Norway, the mountains can cause partial or total beam blocking. Abdella et al. (2012) reported that beam blockage for Hurum radar affects the eastern and south-eastern part of its coverage (Fig. 1) and the beam blockage is up to 30%. Moreover, in high latitude cold climates, non-uniform vertical profile of reflectivity (VPR) and bright band effects in the VPR introduce major uncertainties in the radar precipitation estimation (Abdella, 2016; Koistinen and Pohjola, 2014).

The reflectivity measurements go through a chain of processes to address the above-mentioned errors and uncertainties. The process at met.no first removes clutter and other non-meteorological echoes from the radar scan and then, gaps in the data caused by clutter are reconstructed. After that, volumetric reflectivity data are segmented as a convective or stratiform type of precipitation. Next, the processing algorithm computes VPR according to the precipitation type. To generate SRI product, met.no uses the lowest Plan Position Indicator (PPI). Here, the aloft reflectivity data is projected down to a reference height (1 km) near to the ground and the projection, known as VPR correction that takes variability in the vertical profile of reflectivity (VPR) and bright band effect into account (Elo, 2012). The met.no applies a single Z - R relationship (Marshall and Palmer (1948) relationship, $Z = 200R^{1.6}$) to convert the 7.5 min (or 15 min before June 2013) reflectivities into precipitation rates. The precipitation rates are then accumulated to hourly and distributed as end user hourly radar precipitation rate (SRI) product. The accumulated hourly radar precipitation rate product (SRI product) was used in the present study.

The gauged precipitation data, used in the study, are from the gauges operated by met.no. The met.no undertakes the calibration of gauges and essential measures to reduce the uncertainty in the measurements. Further, met.no performs routine quality control before being released to the data portal for the public. However, met.no does not correct the precipitation data for wind induced undercatch. The precipitation measurements from the gauges are available with varying length as some gauges have been operated since 2013 or later and there are missing values during their operation as well.

Gridded air temperature and wind speed datasets covering Norway are available from met.no. Lussana et al. (2016b) spatially interpolated the past temperature observations from the Norwegian meteorological stations using an Optimal Interpolation in a Bayesian setting to develop a temperature dataset for Norway. The gridded hourly wind speed dataset was derived by statistical downscaling from the 10 km numerical dataset NORA10 combined with the AROME 2.5 km numerical dataset. A local quantile regression method was used for this statistical downscaling. The wind speed data were required in this study to correct wind induced undercatch of gauge precipition.

The datasets for the study were downloaded and prepared as follows. Radar and gauge precipitation and meteorological data (air temperature and wind speed) for the period from January 2011 to May 2015 were used for this study. The gridded hourly radar precipitation rates, air temperature and wind speed data with 1 km × 1 km spatial resolution for the study area were downloaded from met.no's thredds server (http://thredds.met.no/). The gridded data are in netCDF file format in UTM33N projection. The hourly precipitation gauge measurements and gauges meta information were obtained from met.no's data portal "eKlima" (http://eklima.met.no).

The gauge locations were overlaid on the 1 km × 1 km regular grids of the gridded data and the pixel of 1 km^2 overlapping each gauge was located. One location near Oslo has three gauges within a 1 km × 1 km pixel but except for that, all pixels consist of a single gauge. The pixel value for each hour was extracted and continuous hourly time series of radar precipitation rate, air temperature and wind speed for all gauges were generated.

Solid precipitation exhibits significant undercatch due to high wind

conditions in high latitude and mountainous regions (Wolff et al., 2015). In this study, gauged precipitation data were corrected for wind induced undercatch by using the Nordic precipitation undercatch correction model (Førland et al., 1996). The correction model classifies the precipitation phase as solid, liquid and a mixture of two phases using air temperature and the model uses two sets of equations, one for the solid precipitation and other for the liquid precipitation. An average value of the two equations is used for the mixed precipitation. These equations require wind speed and air temperature at gauge location. In this study, the gridded hourly wind speed and air temperature data were used for the undercatch correction. Hereafter, gauge precipitation refers to undercatch corrected precipitation throughout the study.

The precipitation intensities in the study area are relatively low, consistent with intensities in high latitude boreal climates (Sivasubramaniam et al., 2018). A study of statistical properties of precipitation intensities in mid-Norway showed that precipitation rates less than 6 mm h^{-1} yields 88% of the total precipitation volume while less than 1.76 mm h^{-1} yields 50%. Moreover, the same analysis found that precipitation rates below 0.1 mm h^{-1} contributes little to the total precipitation volume and might be regarded as zero precipitation (Engeland et al., 2014). In this study, gauge precipitation and radar precipitation rate less than 0.1 mm h^{-1} were assumed as zero precipitation. At each gauge location, the timesteps with gauge precipitation or radar precipitation rate less than 0.1 mm h^{-1} were removed, and an observed dataset of hourly gauge precipitation and corresponding radar precipitation rate and air temperature was prepared. It can be noted that the length of dataset at each gauge location can vary due to the availability of gauge precipitation records.

To analyse the distribution of gauge and radar precipitation used in this study, observed datasets (gauge and radar precipitation and air temperature) at gauge locations were pooled and histograms were plotted as shown in Fig. 2. Looking at Fig. 2, it is visible that radar underestimates the precipitation compared to gauge observation. Moreover, for intense events, radar precipitation rates show a considerable negative bias for both temperatures colder than and warmer than 10° C. It can be noted that high-intensity hourly precipitation events are rare in the study region. Only 0.03% of the total gauge hours used in the analysis have gauge precipitation intensity above 20 mm h^{-1} while 0.31% have intensity above 10 mm h^{-1}.

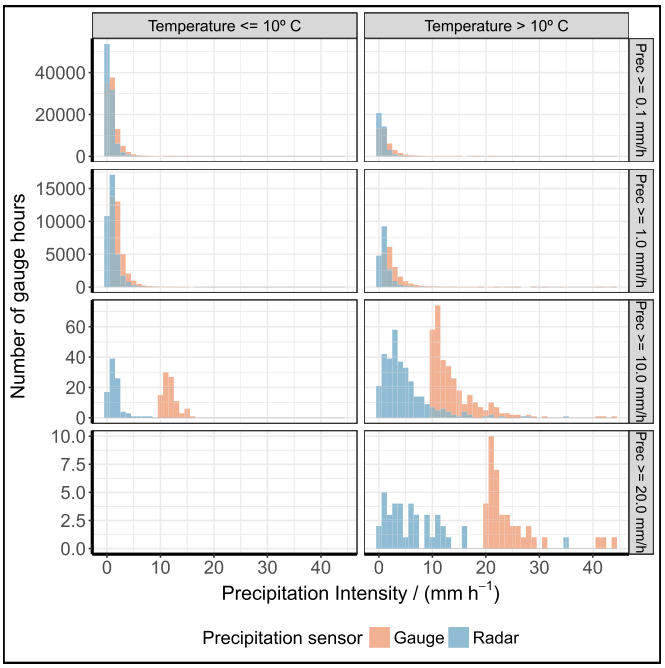

Fig. 2. Histogram representing the distribution of precipitation intensities of gauge and radar precipitation for different threshold precipitation intensities (Prec) of gauge precipitation (0.1, 1.0, 10.0, 20.0 mm h^{-1}) for temperatures colder than and warmer than 10° C. Total gauge hours are nearly 135000 and bin width is 1.0 mm h^{-1}.

In the pooled dataset from the gauge locations, the maximum observed gauge precipitation was 45 mm h^{-1} while maximum radar precipitation rate was 35 mm h^{-1}. However, analysis of radar precipitation rates from the entire set of pixels (46656) showed that there are radar-pixels with extremely high intensity values. A histogram showing the distribution of radar precipitation rates pooled from the entire set of radar-pixels is available in the Supplement (Fig. S1). The intensive values above 50 mm h^{-1} are likely due to hail, or a mixture of very heavy precipitation and hail.

2.3. Methodology

2.3.1. Framework

The two sources of quantitative precipitation from the radar and gauges are combined within a dynamic model combination framework. As an overall description, the flow diagram in Fig. 3 illustrates the data used and the methods applied in the merging process. Merging with gauge precipitation must be applied as the last step in radar precipitation estimation process and all possible corrections should be applied first to improve the radar precipitation estimates before merging (Goudenhoofdt and Delobbe, 2009). The hourly radar precipitation rates were first adjusted within a nonparametric framework using gauge precipitation and air temperature observations (Sivasubramaniam et al., 2018). Since the gauge precipitation data are at gauge locations, a spatial interpolation was applied to get precipitation values at grids. Precipitation values at grids from the two sources were then merged using the estimated combination weights within dynamic model combination framework. Each of the methods is described in detail in the following subsections.

2.3.2. k-nearest neighbour (k-nn) estimation

For the nonparametric estimation, this study adopted the method presented by Sivasubramaniam et al. (2018) for the cold climatological setting where k-nearest neighbour (k-nn) nonparametric model with radar precipitation rate and air temperature as two covariates is used.

Here, a summary of the k-nn method with air temperature as an additional covariate is presented for brevity. More details of the k-nn method of radar precipitation estimation can be found in Sivasubramaniam et al. (2018). Readers are referred to Sharma and Mehrotra (2014); Sharma et al. (2016); Hasan et al. (2016b); Mehrotra and Sharma (2006) for a description of the nonparametric framework.

Conditional estimation of ground precipitation ($R_{est}(t)$) for a given observed pair of radar precipitation rate ($R(t)$)) and air temperature ($T(t)$) using past observed dataset of radar precipitation rate and air temperature and corresponding gauge precipitation within a k-nn regression model is written as follows (Sivasubramaniam et al., 2018).

$$E(R_{est}(t)|[R(t), T(t)]) = \sum_{k=1}^{K} \frac{\frac{g_k}{k}}{\sum_{j=1}^{K} \frac{1}{j}} \quad (1)$$

In Eq. (1), k denotes the number of past observations (radar precipitation rate and air temperature pairs) which are considered similar to the current observation [R, T] and g_k denotes the gauge precipitation corresponding to the k^{th} neighbour in the past observations. K is a maximum number of nearest neighbours permissible and it is taken as equal to the square root of the sample size as recommended by Lall and Sharma (1996). The order of K neighbours is ascertained using a weighted Euclidean distance metric as expressed below.

$$\xi_i^2 = \left(\frac{\beta_R(R - r_i)}{s_R}\right)^2 + \left(\frac{\beta_T(T - t_i)}{s_T}\right)^2 \quad (2)$$

Where, ξ_i is the distance of the current observed pair [R, T] to the i^{th}

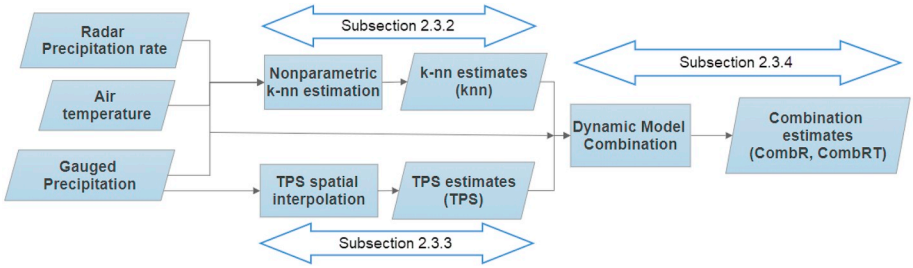

Fig. 3. Flow diagram for the radar and gauge precipitation merging process.

data point (r_i, t_i) in the past observed dataset in a two-dimensional space. s_R and s_T denote sample standard deviations of the two predictors and β_R and β_T are partial weights of predictors and their summation is equal to one. Readers are referred to Sivasubramaniam et al. (2018) for further details about the use of partial weights in k-nn estimation.

The k-nn regression estimator available in the NPRED, R package (Sharma et al., 2016) available for downloading from http://www.hydrology.unsw.edu.au/download/software/npred was used for the nonparametric k-nn estimation in this study. An average partial weight of ($\beta_R = 0.68$, $\beta_T = 0.32$), recommended by Sivasubramaniam et al. (2018) for the study region was used.

A continuous time series of radar precipitation rate and air temperature are on the regular 1 km × 1 km grids. For the k-nn estimation at each pixel (grid) location, the observed dataset (gauge precipitation, radar precipitation rate and air temperature) from the three nearest gauges were pooled and used as past observations with the k-nn regression to estimate precipitation (k-nn estimate). For the timesteps with radar precipitation rate less than 0.1 mm h^{-1}, the k-nn estimates were set as zero.

2.3.3. Thin plate spline (TPS) interpolation

Merging of radar precipitation field with gauges spatially in a regular grid require spatial interpolation of point gauge data. For this study, Thin Plate Splines (TPS) was chosen for the spatial interpolation of gauge precipitation data. It can be noted that for spatially interpolated gauge precipitation to use in the combination method, any of the interpolation techniques as listed in section 1 can be used if the estimates of variance in the fitted precipitation surface are available (Hasan et al., 2016b).

The TPS interpolation is a data driven nonparametric approach of locally weighted polynomial method. The optimal number of neighbours around each target is determined using general cross validation (GCV) statistics (Hwang et al., 2012). A number of studies (Hutchinson, 1998a, b; Tait et al., 2006; Woldemeskel et al., 2013) have reported the application of TPS method for spatial interpolation of gauge precipitation. “Tps” from the R package (library) “fields v9.0” (Nychka et al., 2017) available on the Comprehensive R Archive Network (CRAN) was used to fit a thin plate spline precipitation surface from precipitation gauges in this study. A description of the “Tps” can be found in the R documentation (https://www.rdocumentation.org/packages/fields/versions/9.0/topics/Tps). In the “Tps”, the smoothing parameter is chosen by generalized cross validation.

2.3.4. Dynamic model combination

At each pixel (1 km × 1 km grid), we have spatially estimated k-nn radar precipitation estimates using a model with radar precipitation rate and air temperature as two predictor variables (k-nn) for each hourly timestep. We also interpolated gauge precipitation using TPS to provide an alternate estimate that uses a different data source. As a result, all 46656 pixels in the study area have continuous time series of k-nn and TPS estimates.

The k-nn and TPS estimates have different estimation accuracy. The estimation accuracy varies spatially from one pixel location to another as well as temporally at a given pixel location. Within a model combination framework, the two estimates can be combined by weighting each method according to their past observed estimation accuracy (Bates and Granger, 1969; Wasko et al., 2013; Hasan et al., 2016b).

In this study, the combination weight of each method is calculated from the error covariance matrix using residual errors corresponding to past observations. To calculate the error, we need a true observation of the estimated precipitation value. At pixel locations coinciding with gauges, corresponding gauge precipitation was taken as the true precipitation and k-nn and TPS errors were calculated. This study used the leave one out cross validation (LOOCV) procedure to calculate these errors. The k-nn error at a gauge location was calculated by leaving out one observed response (gauge precipitation) from the k-nn regression and estimating the expected response value for that observed response to obtain the error for each observation. A matrix of observed gauge precipitation and corresponding precipitation rate and air temperature and k-nn error (e_{k-nn}) was generated at each gauge location.

TPS error was calculated using spatial LOOCV whereby leaving a gauge from spatial interpolation and estimating the TPS response for each observed precipitation value allowed TPS error to be calculated with reference to the observed precipitation value. TPS error matrix with observed precipitation and corresponding TPS error (e_{TPS}) was generated. The k-nn error matrix and TPS error matrix were next merged to obtain an error matrix of radar precipitation rate and air temperature and corresponding k-nn error (e_{k-nn}) and TPS error (e_{TPS}) at 87 gauge locations.

To merge the TPS and k-nn estimates, combination weights were calculated at each pixel (grid) location (x, y) for each hourly time step (t) as described follows. Each pixel can be associated with a radar precipitation rate ($R_{x,y}(t)$), air temperature ($T_{x,y}(t)$) and corresponding precipitation estimates using TPS ($P_{TPS,x,y}(t)$) and k-nn ($P_{k-nn,x,y}(t)$). To estimate the combination weight, error matrices from three nearest gauges for this pixel were pooled. The pooled error matrix $Y = [R_{x,y}, T_{x,y}, e_{k-nn,x,y}, e_{TPS,x,y}]$ consist of radar precipitation rate, air temperature and corresponding estimated k-nn and TPS error from past observations.

The static combination approach uses entire observations to estimate error covariance matrix at a given pixel location. In contrast, the dynamic combination identifies a number of similar precipitation events to estimate error covariance matrix for each timestep at the pixel location. Here the k-nearest neighbour (k-nn) method with a Euclidean distance metric was used to ascertain the neighbours and the number of maximum neighbours was equal to the square root of the sample size as recommended by Lall and Sharma (1996).

Hasan et al. (2016b) identified similar events using reflectivity as a single variable. In contrast to their approach, this study uses radar precipitation rate and air temperature as two variables to identify similar events using k-nearest neighbour technique in the dynamic model combination algorithm to merge k-nn and TPS estimates. The proposed combined product of k-nn and TPS is denoted as P_{CombRT}. For comparison, a reference model combination of k-nn and TPS estimates using radar precipitation rate as a single variable to identify similar events in the dynamic model combination algorithm, as similar to Hasan et al.

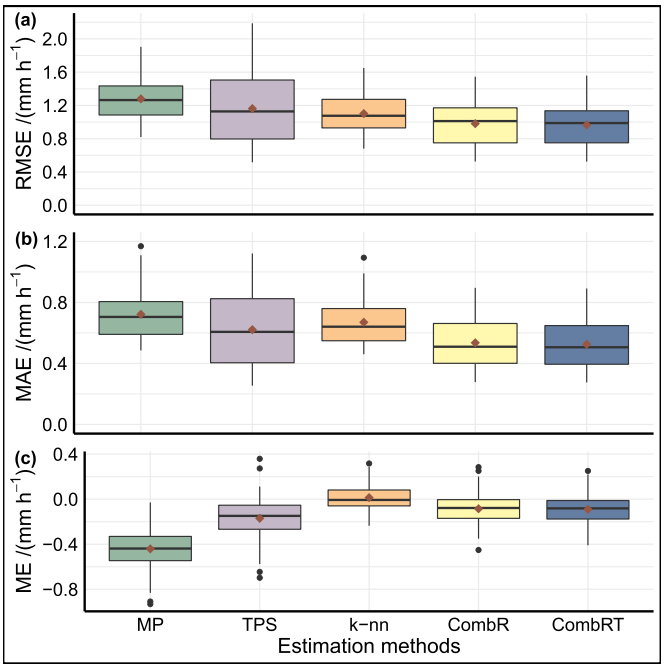

Fig. 4. Box plot representing a summary of performance metrics (RMSE, MAE and ME) at 87 gauge locations for the radar precipitation rates (MP), Thin Plate Spline interpolation (TPS), k-nearest neighbour estimates (k-nn) and the combination (CombR and CombRT). Mean value of the performance metric for each model is marked with a red diamond. The values outside 1.5*IQR are represented by the whiskers. (For interpretation of the references to colour in this figure legend, the reader is referred to the Web version of this article.)

(2016b) were also developed (P_{CombR}).

For each time step, for the given radar precipitation rate and air temperature pair at the pixel location $[R_{x,y},\ T_{x,y}](t)$, k number of similar $[R,\ T]$ pairs from the past observations in the matrix Y were identified and hence corresponding k number of k-nn error (e_{k-nn}) and TPS error (e_{TPS}) pairs were selected. In the reference model, for the given radar precipitation rate $[R_{x,y}](t)$, k number of similar [R] from the matrix Y were identified to select k-nn and TPS error pairs.

An error covariance matrix ($\sum e$) of the estimation errors was calculated for the selected error pairs $[e_{k-nn},\ e_{TPS}]$ and the covariance matrix can be written as follows.

$$\sum e = \begin{bmatrix} \sigma^2_{TPS} & \rho\sigma_{TPS}\sigma_{k-nn} \\ \rho\sigma_{TPS}\sigma_{k-nn} & \sigma^2_{k-nn} \end{bmatrix} \tag{3}$$

Here diagonals are the variance of the errors of each method and off diagonals represent covariance of the errors from the two methods. Where, ρ is the correlation between errors from the two estimation methods.

The dynamic combination weight of the two estimates can be calculated by minimizing the quantity as shown in (4) such that the weights being constrained to lie between 0 and 1 and their summation is unity (Khan et al., 2014; Hasan et al., 2016b). For further details of the derivation of Eq. (4), readers are referred to Khan et al. (2014).

$$\min\left(W' \sum_e W\right) \tag{4}$$

Here, $W' = [W_{TPS},\ W_{k-nn}]$ and the summation ($W_{TPS} + W_{k-nn}$) is equal to 1. W_{TPS} denotes the combination weight associated with TPS estimates while the weight associated with k-nn is denoted by W_{k-nn}.

The combined precipitation estimation ($P_{CombRT,x,y}(t)$) is the weighted summation of k-nn and TPS estimates as follows

$$P_{CombRT,x,y}(t) = W_{k-nn}P_{k-nn,x,y}(t) + W_{TPS}P_{TPS,x,y}(t) \tag{5}$$

At pixel locations coinciding with gauges, the estimates were obtained using leave one out cross validation (LOOCV). The LOOCV ensures the modelled outcomes (P_{k-nn}, P_{TPS}, P_{CombR} and P_{CombRT}) are obtained from independent of gauge precipitation values those will be used to evaluate the modelled outcomes. The k-nn estimate was calculated by leaving out the current radar precipitation rate and air temperature and corresponding gauge precipitation from the past observed dataset in the k-nn regression. The TPS estimate was obtained by leaving a gauge from spatial interpolation and estimating the TPS response on that gauge location. To calculate the weight for each timestep in the dynamic combination, the error covariance matrix was formulated by excluding the k-nn and TPS error pair corresponding to the current k-nn and TPS estimates.

2.3.5. Model evaluation criteria

Several performance metrics have been used in literature to assess the performance of the models and compare them (Villarini et al., 2008; Hasan et al., 2016b). Some of the metrics are root mean square error (RMSE), mean absolute error (MAE) and mean error (ME). The RMSE provides the overall performance measure of a predictive model (Hasan et al., 2016b). The study primarily used the RMSE as a performance metric to evaluate the model performance. To strengthen the evaluation, additional performance metrics, MAE and ME, were also used. Definition of the performance metrics used in this study can be found in the published literature (Villarini et al., 2008; Bennett et al., 2013; Hasan et al., 2016b).

3. Results

3.1. Performance of dynamic combination

The performance of the modelled outcomes was evaluated at gauge locations. For the assessment, we computed performance metrics (RMSE, MAE and ME) for the k-nn, TPS and the combination estimates (CombR and CombRT) at 87 gauge locations for the timesteps with radar precipitation rate and gauge precipitation greater than 0.1 mm h^{-1}. Here, gauge precipitation was taken as a true observed value to compute the performance metrics. The performance metrics were also estimated for radar precipitation rates, which was considered as a benchmark to compare the modelled estimates.

Fig. 4 shows a comparison of performance metrics computed at 87 gauge location for the precipitation estimates using different estimation methods and for the radar precipitation rates (MP). The Nonparametric k-nn estimation (k-nn) leads to a considerable decrease in the RMSE in the radar precipitation estimates. The merging of k-nn and TPS estimates within a dynamic model combination framework reduces the RMSE in the estimated precipitation field significantly. The mean improvement in RMSE for k-nn is 15.0% (from 1.3 to 1.1 mm h^{-1}) while it is over 25% (1.3–0.95 mm h^{-1}) for the proposed dynamic model combination estimation (CombRT) compared to the radar precipitation rates. Further, almost all gauge locations exhibited clear improvement in estimates using dynamic combination approach.

Looking at Fig. 4, TPS estimates has a relatively smaller error than radar precipitation rates (MP). This displays the errors associated with the radar precipitation. It can be noted that TPS interpolation technique was the method of choice in this study and the focus of the study was not to assess the different interpolation methods to select for the model combination. As shown in Fig. 4 (c), the mean error (ME) of the radar precipitation rates (MP) which represents the bias in the MP, was negative for almost all gauge locations. This demonstrates the underestimation of radar precipitation compared to gauge precipitation. The k-nn estimation noticeably reduces the bias (ME) in the radar precipitation to near zero (from −0.44 to 0.01 mm h^{-1}) while reducing the RMSE and MAE.

Most of the gauge locations showed clear reduction in RMSE and MAE in the precipitation estimates by merging the two sources than the

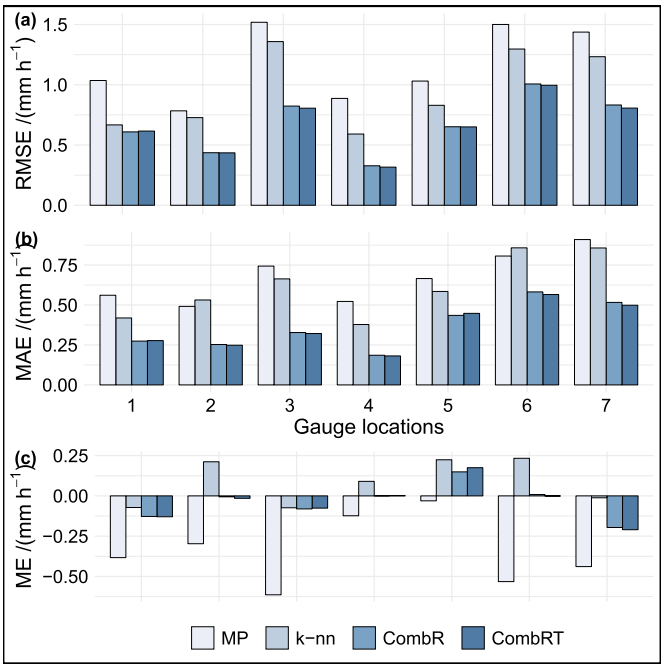

Fig. 5. Bar plot representing three performance metrics (RMSE, MAE and ME) estimated at 7 control gauge locations for the radar precipitation rates (MP), k-nearest neighbour (k-nn) and the combination estimates (CombR and CombRT).

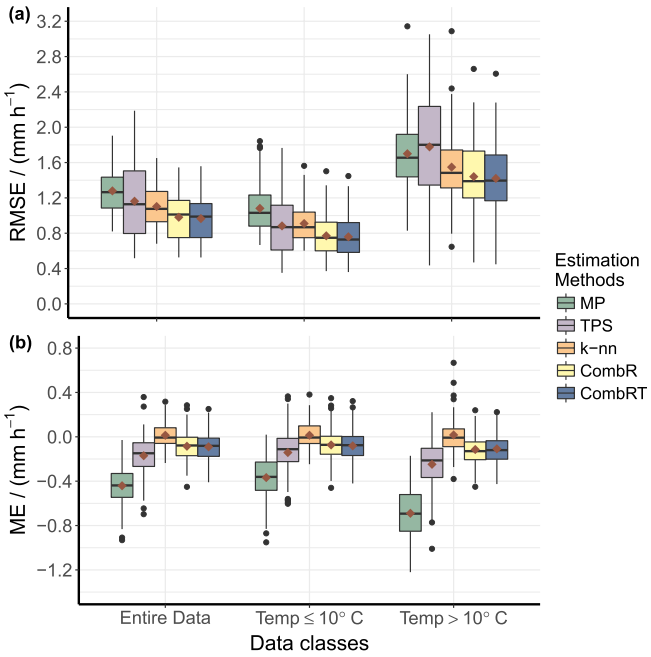

Fig. 6. Box plot of RMSE and ME (mm h^{-1}) values estimated at 87 gauge locations for the radar precipitation rates (MP), TPS interpolation (TPS), k-nn estimation (k-nn) and the combination methods (CombR and CombRT) using entire data and dataset with temperatures colder than or equal 10° C and warmer than 10° C. Mean value of RMSE and ME for each model is marked with a red diamond. The values outside 1.5*IQR are represented by the whiskers. (For interpretation of the references to colour in this figure legend, the reader is referred to the Web version of this article.)

estimation (k-nn or TPS) using the data from a single sensor (radar or gauge). However, the ME associated with combination estimation (mean value of - 0.1 mm h^{-1}) was slightly higher than k-nn estimation while it is less than the TPS estimates (mean value of - 0.2 mm h^{-1}). The proposed merging method using air temperature as an additional variable in the dynamic combination algorithm (CombRT) slightly improves the precipitation estimates compared to the reference model (CombR). Looking at Fig. 4, the improvement is not very high. However, more than 80% of the gauge locations, RMSE of CombRT is lower than CombR.

In addition, we also evaluated the estimates at the 7 independent gauge locations to verify the results on ungauged pixel locations. The gauge precipitation data from those control gauge locations have not been used in any of the estimations. We found a similar result at these control gauge locations as for the study gauges. A bar plot representing these performance metrics at 7 control gauge locations is shown in Fig. 5.

While Fig. 4 presents the summary of performance metrics for the 87 gauges obtained by using LOOCV procedure, the values of performance metrics estimated for each of those 7 control gauges are presented in Fig. 5. The combination approach reduces the RMSE and MAE for all seven-gauge locations while it decreases the ME in the radar precipitation rates for most of them and it resembles the summary result presented in Fig. 4. Looking at Fig. 5, the magnitude of the performance metrics varies among gauges. We investigated whether they are due to beam blockage. However, we could not find any spatial pattern in the magnitude of the errors at gauge locations. Here it can also be noted that, the data length at each gauge location is not the same as mentioned in section 2.2.

3.2. Variation with temperature classes

To investigate whether the improvement can vary with temperature ranges, we computed performance metrics for the datasets with temperatures colder than or equal and warmer than 10° C and RMSE and ME are shown in Fig. 6. Looking at Fig. 6 (a), for temperatures colder than or equal 10° C, radar precipitation (MP) have a higher RMSE than the TPS interpolation. This shows that the radar performance is poorer for colder temperatures than warmer. There are relatively higher errors and uncertainties in the radar measurement of precipitation in cold temperatures. For temperatures warmer than 10° C, the overall RMSE is higher for TPS than for radar precipitation. This can be due to TPS spatial interpolation of gauge precipitation using available sparse gauges resulting in more error. This is turn could be due to such events being local convective events where radars perform better.

Fig. 6 (b) shows the estimated bias (ME) in the different estimation for the two temperature classes. Radar precipitation rates (MP) have substantial negative bias (under estimation) for both colder and warmer temperatures. It can be noted that met.no uses the single Z - R relationship (Marshall and Palmer (1948) relationship for rain) to convert the reflectivities to precipitation rates. An inappropriate relationship (Z - R relationship for rain instead of snow) in the conversion can also result in phase dependent bias in the estimation for colder temperatures. Similar argument can be valid for the bias in the radar precipitation for temperatures warmer than 10° C, where the single Z - R relationship cannot be appropriate for different types of rainfall (orographic or convective) as they have different raindrop size distribution (Uijlenhoet, 2001). The nonparametric k-nearest neighbour (k-nn) estimation reduces the bias in the radar precipitation for both temperature classes.

Looking at Fig. 6 (b), TPS interpolation of gauge precipitation also resulted in negative bias at most of the gauge locations, but it is considerably less than the bias in the radar precipitation. For both estimates, the magnitude of the bias is higher for warmer temperatures than colder; this is because precipitation intensities of colder temperatures are relatively low and the values in the plot is not normalised. The bias in the merged precipitation (CombR and CombRT) is lower than TPS estimates; however, it is slightly higher than the k-nn estimates.

The nonparametric k-nearest neighbour model (k-nn) reduces the

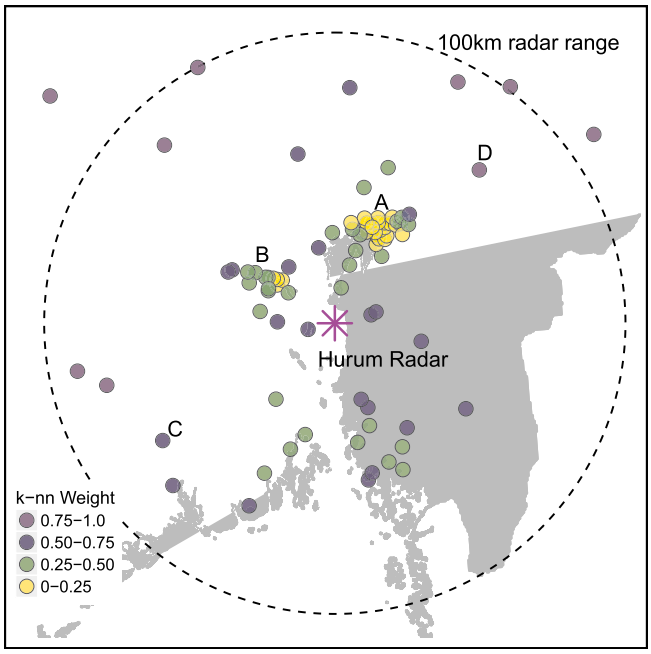

Fig. 7. Spatial variation of combination weight of k-nn estimates at 87 gauge locations, overlaid on the coastline and Norway-Sweden border in the study area. Discrete filled colour represents the weights assigned to k-nn and the summation of weights is equal to 1 ($W_{k-nn} + W_{TPS} = 1$). (For interpretation of the references to colour in this figure legend, the reader is referred to the Web version of this article.)

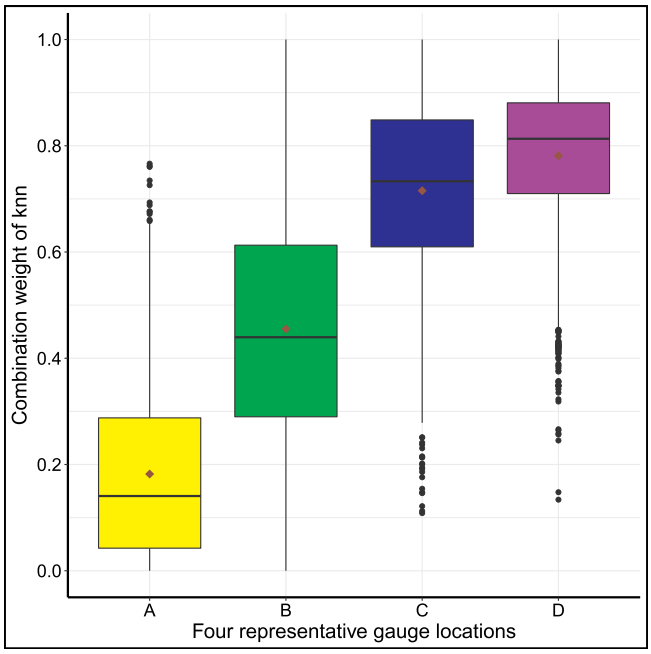

Fig. 8. Variation of combination weight of k-nn at four gauge locations, "A″, "B″, "C″ and "D″ as shown in Fig. 7. Filled colour represents the average weight range as in the legend of Fig. 7 in which these location's average weight resulted in. The mean value of the weight is marked with a red diamond. The values outside 1.5*IQR are represented by the whiskers. (For interpretation of the references to colour in this figure legend, the reader is referred to the Web version of this article.)

RMSE in the radar precipitation estimation significantly for temperatures colder than 10° C. The k-nn estimation still improves the radar precipitation estimation for warmer temperatures also. Both combination methods (CombR and CombRT) significantly reduces the RMSE compared to any of the other estimations for both temperature classes. For temperatures colder than 10° C, the use of air temperature in the dynamic combination algorithm (CombRT) results in marginal improvement compared to the reference model without air temperature (CombR) and the performance is nearly same for temperatures warmer than 10° C.

3.3. Combination weights

As mentioned earlier, combination weights vary with space and time. The dynamic assignment of weight ensures the provision of merit to the best method in the combination at any location for any particular time step (Hasan et al., 2016b). To comprehend the usefulness of dynamic model combination approach, the spatiotemporal variation of combination weights was scrutinized.

Fig. 7 shows the spatial plot of combination weight associated with k-nn at 87 gauge locations in the study area. The circles represent the gauge locations and a discrete filled colour scale is used to show the combination weights assigned to k-nn estimates. It can be noted that the summation of weights ($W_{k-nn} + W_{TPS}$) is equal to 1.

It is clearly visible from Fig. 7 that, k-nn gets lower weight (yellow filled circles) and hence TPS gets more weight at densely gauged locations while k-nn gets higher weight in the low density regions. The circles filled with blue colour represents the gauged pixel locations where the k-nn gets equal or higher weight compared to TPS. In the northern and western boundary of the study area with sparse gauges, the highest average weight of more than 0.75 was assigned to the k-nn estimates. The result is consistent with (Hasan et al., 2016b) where they used a denser gauge network (282 tipping bucket gauges).

Fig. 7 shows the average combination weight for the entire time-steps at each gauge location. In addition to spatial variation, at any pixel location, the combination weights also vary with time. In this paper, we illustrate the temporal variation for the four-gauge locations which are marked with "A″, "B″, "C″, "D″ in Fig. 7 and the temporal variation is shown using a box and whisker plot in Fig. 8. The locations were chosen to represent the four classes of combination weight as listed in the legend of Fig. 7.

The location "A″ is in a densely gauged area and "B″ is from a less dense gauged area while "C″ and "D″ are in a sparse gauged region. Looking at Fig. 8, the resulting combination weights of k-nn are in a range of values between 0 and 1 for all four locations. For the locations "A″ and "B″, the average weight of k-nn is less than 0.5, but a number of hourly events still get a weight above 0.5 for k-nn and vice versa for the locations "C″ and "D". The dynamic model combination method assures the best data source (k-nn or TPS in this case) is chosen in the combination for each hourly event.

The proposed dynamic model combination uses air temperature as an additional variable to identify similar events to estimate the combination weight. Fig. 9 illustrates the variation of combination weight assigned to the two estimates for the datasets with temperatures colder and warmer than 10° C at the gauge locations. Looking at Fig. 9, radar based k-nn estimaton gets a relatively less weight than TPS for air temperatures colder than 10° C. For temperatures warmer than 10° C, the k-nn estimates get a higher average weight than TPS for more than 50% of the gauge locations. The overall aggregated average weight for k-nn is 0.43 while 0.57 for TPS.

3.4. Analysis of high-intensity storm events

Fig. 10 shows a histogram of radar and gauge precipitation and resulting estimates (k-nn and combination) for high-intensity hourly events at the gauge locations. Looking at Fig. 10, nonparametric k-nn estimation results in lower estimation for the intensive events observed by gauges. This can be because of lack of data points with intensive events in the past observed dataset. To ascertain accurate estimates

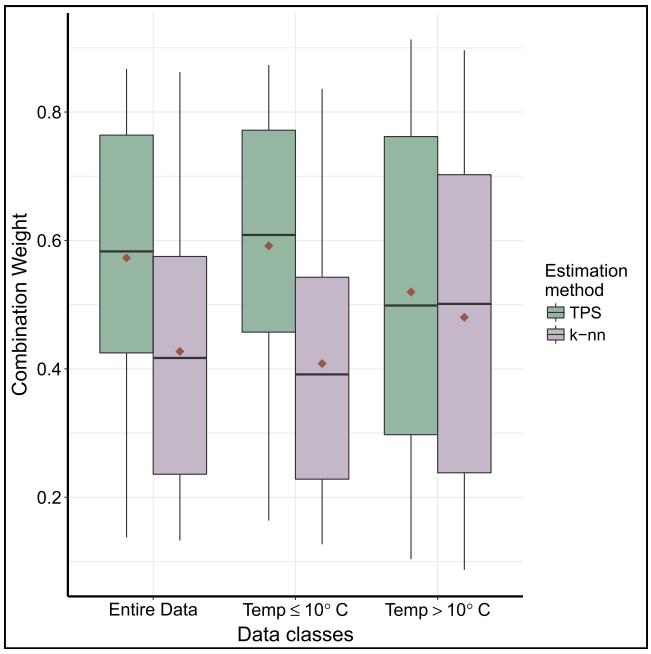

Fig. 9. Variation of combination weight assigned to k-nn and TPS estimates at 87 gauge locations for temperatures colder than or equal and warmer than 10° C. Mean value of weight is marked with a red diamond. Here, $W_{k-nn} + W_{TPS} = 1$. (For interpretation of the references to colour in this figure legend, the reader is referred to the Web version of this article.)

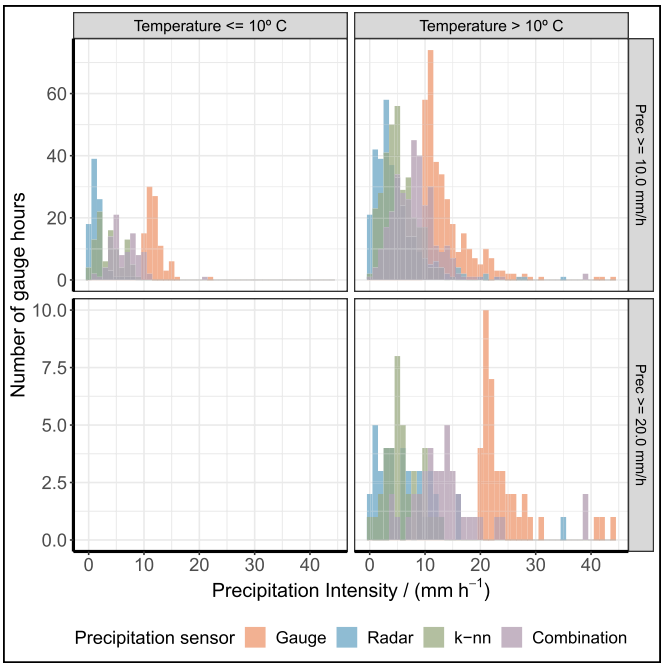

Fig. 10. Histogram representing the distribution of gauge and radar precipitation intensities and the k-nn and combination estimates at gauge locations for precipitation intensities (Prec) of gauge precipitation above 10 mm h^{-1} and 20 mm h^{-1} for temperatures colder and warmer than 10° C. Bin width is 1.0 mm h^{-1}.

using a nonparametric method that is based on local regression, enough number of past observations with similar intensities are required (Hasan et al., 2016b). The combination improves the precipitation estimates; however, combination estimates are also still lower than the gauge precipitation for higher precipitation rates.

To assess the modelled outcomes for individual storm events,

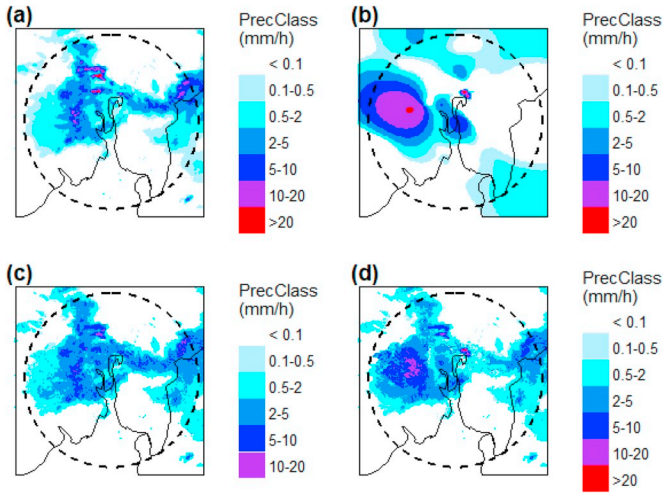

Fig. 11. Precipitation estimation for an hourly storm event on 26 June 2014 at 15:00 UTC from a) radar precipitation rates b) TPS, c) k-nn, d) CombRT. The spatial hourly air temperature was in the range 6° C - 19° C.

resulting raster images were made in order to visually inspect the usefulness and limitations of the different precipitation estimation methods. The event shown in Fig. 11 was one of the recorded extreme hourly summer events by the gauging stations in Oslo. The spatial air temperature in the study area during the hourly event was in the range of 6° – 19° C over the pixels. Looking at Fig. 11, both radar and gauges (TPS) observed the local extremes and shows pixels with high intensities. Comparing Fig. 11(a) and (b), radar displays several pixels with intense precipitation while TPS displays extremes at two locations. Further, radar shows precipitation on the eastern part of the study area but TPS did not show any precipitation because of very sparse gauges in this area and they could therefore not capture the event. The advantage of extended spatial coverage of radar is clearly visible from this event. Spatial interpolation generally smooths out the spatial variation as it is visible on Fig. 11(b). Looking at Fig. 11(c), the k-nn did not show any high intense values (intensity greater than 20 mmh^{-1}). As described above, if there are no similar intensive events in the past observations, the k-nn local regression estimation can result in underestimation.

The merging of k-nn and TPS estimates brought the quantitative information partially from gauges and radar while it reflects the spatial variation detected by radar in the resulting image of the combination estimate as shown in Fig. 11 (d). The radar image (Fig. 11 (a)) shows the pixels with high intense values in the northwest and northeast part of the study area; however, the resulting image in the combination does not display them as intense. The more useful information from a radar is the spatial distribution of precipitation. The usefulness of combination approach is demonstrated at the eastern part where the combination resulted in precipitation even though TPS did not show any precipitation there.

Winter precipitation intensities are relatively low in the study region, consistent with intensities in boreal climates. To compare the estimation methods for a winter event, a 6-h winter storm event on 26 March 2015 is selected to present. It can be noted that the gauges observed nearly similar hourly intensities during the 6-h period. The hourly precipitation estimates using different estimation methods on 1 km × 1 km pixels for the period from 06:00 to 11:00 UTC were accumulated and displayed in Fig. 12. This winter storm disturbed the transport and other essential functions in the capital city, Oslo and neighbouring areas.

Looking at Fig. 12, accumulated radar precipitation was very low. As shown in the aggregated results in Fig. 4, radar underestimates the precipitation. However, it shows better the spatial variation in the precipitation. The TPS interpolation smooths out the spatial variation

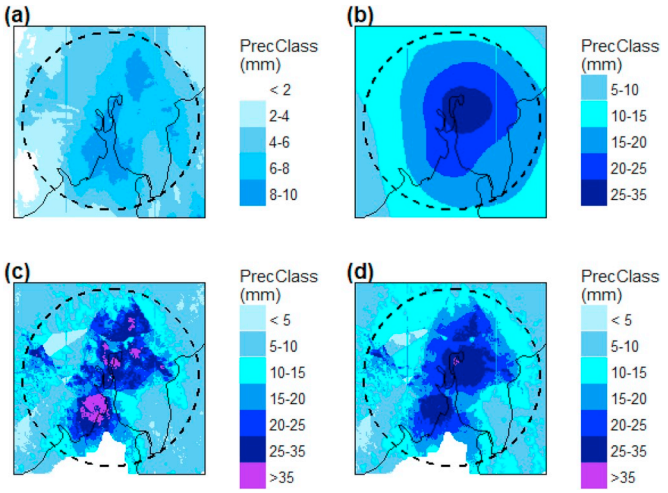

Fig. 12. Precipitation estimation for a 6-h winter storm event on 26 March 2015 from 06:00 to 11:00 UTC. Accumulated hourly estimates using a) radar precipitation rates b) TPS, c) k-nn, and d) CombRT. The spatial average air temperature was in the range −10° C - 1° C.

based on the available gauges observations. The k-nn estimates show higher precipitation than the TPS interpolated values. The nonparametric k-nn estimation is based on the local regression of past similar observations. It can be noted that, the k-nn estimation using air temperature as an additional covariate ascertains similar cold events as the nearest neighbours if such events in the past observations. Fig. 12 (d) shows the resulting image of the accumulated hourly estimates of the combination of TPS and k-nn. The combination resembles the spatial variation shown in the k-nn estimation, however; it did not show higher precipitation for many pixels as in the k-nn. The dynamic combination approach provides more weight to the method with less error in the past estimation. For this winter event, the quantitative estimation from the radar (k-nn) gets less weight than the estimation derived from gauges (TPS) on these pixels.

4. Discussion

Water resources engineering and hydrological studies on a catchment scale are often limited by high spatiotemporal precipitation estimates available (Syed et al., 2003; Smith et al., 2004; Hailegeorgis et al., 2016). In cold climates, precipitation estimation using available sensors (both gauges and radars) are confronted with an additional challenge of phase dependent uncertainties (Saltikoff et al., 2015; Wolff et al., 2015). The precipitation measurements by gauge network and weather radar have their own merits and shortcomings. It is often shown that merging the two sources can result in improved precipitation estimates (Haberlandt, 2007; Berndt et al., 2014; Hasan et al., 2016b). In this study, we combined the two precipitation data sources by taking advantage of their merits and rectifying their shortcomings. The combination approach considerably decreased the negative bias in the radar precipitation while it reduced the mean squared error by one-fourth of the errors associated with the original hourly radar precipitation rates. As a result, we generated an improved continuous hourly time series of gridded (1 km × 1 km) precipitation for the area with a radar coverage of radius 100 km.

This study has formulated a framework which adopted a nonparametric estimation model and a dynamic model combination approach to merge radar and gauge precipitation in cold climates. In a typical radar-gauge merging process, radar precipitation rates from the processing chain (clutter cancellation, VPR correction and Z - R conversion) are directly used for merging. Analysis of data showed that the radar precipitation rates have a noticeable bias, including phase dependent bias. In contrast to the traditional approach, this study first adjusts the radar precipitation rates using the nonparametric k-nn method before merging with gauge precipitation, otherwise the bias could remain in the merged precipitation estimates.

We employed the nonparametric k-nn method with air temperature as an additional covariate to adjust the radar precipitation for colder temperature conditions, and then also for use within the dynamic model combination. The use of air temperature in the dynamic model combination algorithm did not result in an improvement similar to the nonparametric estimation in Sivasubramaniam et al. (2018). However, the proposed method marginally improved the estimates compared to the combination using radar precipitation rate alone. When gridded air temperature data are available, the use of air temperature in the dynamic model combination algorithm is inexpensive and that results in added value to the resulting precipitation estimates in cold climates.

Geostatistical merging methods consider radar precipitation as a secondary information to improve spatially interpolated gauges (Goudenhoofdt and Delobbe, 2009; Rabiei and Haberlandt, 2015). In contrast to those merging methods, the dynamic variation of the weight in the model combination takes intensity information from radar precipitation as a potential source of equal importance to gauge precipitation. The model combination approach can be more useful for a relatively less dense gauged area where quantitative information from the radar can be more accurate than the interpolated gauge value.

The results of the dynamic model combination found are comparable with the results of Hasan et al. (2016b). In this study, the dynamic model combination framework of Hasan et al. (2016b) for a tropical setting was extended to a Norwegian cold climatological context. Compared to Hasan et al. (2016b) univariate (radar reflectivity as a single variable) kernel based nonparametric estimates, this study employed a bivariate nonparametric k-nearest neighbour model with radar precipitation rate and air temperature as two covariates to adjust the radar precipitation rates first. Further, a Thin Plate Spline (TPS) was applied to spatially interpolate the gauge precipitation data to regular grids. Finally, air temperature was used as an additional variable to find similar events to estimate the dynamic combination weights. However, in contrast to Hasan et al. (2016b), this study aims to generate continuous hourly time series of improved radar based precipitation field for the region, which can be readily useable with hydrological models.

Hasan et al. (2016b) tested the combination method over the Sydney region in Australia and reported that the nonparametric estimation reduced the RMSE in rainfall estimates by 10% and the model dynamic combination reduced by 20% compared to radar as a single sensor using a parametric Z - R relationship. In this study, nonparametric k-nn estimation resulted in a mean reduction in RMSE of 15% while a mean reduction in RMSE of 25% was obtained using the dynamic combination method. Further, Hasan et al. (2016b) reported that the bias in parametric and nonparametric estimation was the same. In contrast, k-nn estimation in this study resulted in a considerable reduction in bias. The reason can be due to that Hasan et al. (2016b) used a gauge adjusted parametric relationship for the study region and compared with nonparametric estimation, while precipitation rates used in this study were estimated by met.no using Marshall and Palmer (1948) relationship without any gauge adjustment.

Work at the Norwegian Meteorological Institute (met.no) with the same objective is currently underway. An experimental release from met.no on this work reported merging of hourly radar precipitation rates with disaggregated daily gauged precipitation to hourly data using an optimal interpolation method (Lussana et al., 2016a). In contrast, the present study merged the nonparametric estimation of radar precipitation with interpolated hourly gauge precipitation. The findings from the present study can be an input for the ongoing Norwegian national project of developing gridded radar-based precipitation field.

The improved continuous hourly precipitation field obtained through the combination process can be a readily available data source for hydrological applications. Radar precipitation data have relatively smaller number of missing observations; in addition radar covers a

large geographical area. However, the radar precipitation field has relatively high errors; these errors can potentially bias the calibration of hydrological models and water balances computations (Oke et al., 2009). The current study exploited the advantages inherited in the radar data while it reduced the root mean squared error as well as the negative bias in the original radar precipitation field. As a result, improved continuous precipitation data are becoming available on the catchment scale for many small catchments. The high spatial precipitation field could solve issues related to precipitation representativity of catchment scale hydrological modelling (Syed et al., 2003; Smith et al., 2004; Kirchner, 2009). Further, the resulting long-term continuous precipitation estimates can be led for deriving radar-based climatology of precipitation for the region as similar to Overeem et al. (2009). The use of data with hydrological models to simulate the river flow and snow accumulations and reconstruct the extreme events would be an immediate and interesting next step for this work.

5. Conclusions

The study developed a method to merge the radar and gauge precipitation observations, further, investigated the usefulness of air temperature as an additional factor in the combination process in cold climates.

An improvement of 25% in the root mean squared error was obtained using the dynamic model combination method compared to the original radar precipitation rates. Almost all gauge locations, where we evaluated the modelled outcomes, showed a significant improvement in the precipitation estimation. Air temperature as an additional variable in the combination algorithm marginally improve the precipitation estimates compared to the algorithm without air temperature. However, the improvement was not high as it yielded for the non-parametric estimation in cold climates.

Given the need for high spatiotemporal precipitation data on the catchment scale and the availability of resulting data in remote areas in a continuous setting because of radar's extended coverage, the above finding could be useful for practical hydrology.

Software and data availability

Radar precipitation rate data used in the study are available in the Norwegian Meteorological Institute's (met.no) thredds server (http://thredds.met.no/thredds/catalog/remotesensingradaraccr/catalog.html). Gauge precipitation data and gauges' meta information can be obtained from met.no's web portal eKlima (http://eklima.met.no) and access to the web portal is available upon request. Gridded hourly air temperature and wind speed data are obtained from met.no's thredds server (http://thredds.met.no/thredds/catalog.html). NPRED programming tool is available as R package and it can be downloadable from the following link as follows: http://www.hydrology.unsw.edu.au/download/software/npred. The R package “fields v9.0″ is available on the Comprehensive R Archive Network (CRAN) to install.

Competing interests

The authors declare that there are no competing interests.

Acknowledgements

The authors thankfully acknowledge the Norwegian meteorological institute (met.no) for providing radar and gauge precipitation and meteorological data for this study. The authors would like to thank Christoffer Artturi Elo and Cristian Lussana at met.no for the assistance to get the gridded radar precipitation and meteorological data. A great appreciation goes to Water Research Centre, University of New South Wales (UNSW), Sydney, Australia for hosting the first author for research practicum. The authors gratefully acknowledge the Norwegian Research Council and Norconsult for funding this research work under the Industrial Ph.D. scheme (Project No.: 255852/O30).

Appendix A. Supplementary data

Supplementary data to this article can be found online at https://doi.org/10.1016/j.envsoft.2019.05.013.

References

Abdella, Y., 2016. Quantitative Estimation of Precipitation from Radar Measurements: Analysis and Tool Development. Ph.D. thesis. Norwegian University for Science and Technology, Trondheim.

Abdella, Y., Engeland, K., Lepioufle, J.M., 2012. Evaluation of Radar-Derived Precipitation Estimates Using Runoff Simulation: Report for the NFR Energy Norway Funded Project ”Utilisation of Weather Radar Data in Atmospheric and Hydrological Models. Technical Report. SINTEF Energy Research, Trondheim, Norway.

Al-Sakka, H., Boumahmoud, A.A., Fradon, B., Frasier, S.J., Tabary, P., 2013. A new fuzzy logic hydrometeor classification scheme applied to the French x-, c-, and s-band polarimetric radars. J. Appl. Meteorol. Climatol. 52, 2328–2344.

Auer Jr., A.H., 1974. The rain versus snow threshold temperatures. Weatherwise 27 67–67.

Bates, J.M., Granger, C.W., 1969. The combination of forecasts. J. Oper. Res. Soc. 20, 451–468.

Bennett, N.D., Croke, B.F., Guariso, G., Guillaume, J.H., Hamilton, S.H., Jakeman, A.J., Marsili-Libelli, S., Newham, L.T., Norton, J.P., Perrin, C., et al., 2013. Characterising performance of environmental models. Environ. Model. Softw 40, 1–20.

Berndt, C., Rabiei, E., Haberlandt, U., 2014. Geostatistical merging of rain gauge and radar data for high temporal resolutions and various station density scenarios. J. Hydrol. 508, 88–101.

Berne, A., Krajewski, W.F., 2013. Radar for hydrology: unfulfilled promise or unrecognized potential? Adv. Water Resour. 51, 357–366.

Beven, K., 2012. Data for rainfallrunoff modelling. In: Rainfall-Runoff Modelling: the Primer, 2 ed. John Wiley & Sons, Ltd, Chichester, UK, pp. 51–82. https://doi.org/10.1002/9781119951001.ch3. (chapter 3).

Brandes, E.A., 1975. Optimizing rainfall estimates with the aid of radar. J. Appl. Meteorol. 14, 1339–1345.

Chowdhury, S., Sharma, A., 2009. Long-range niño-3.4 predictions using pairwise dynamic combinations of multiple models. J. Clim. 22, 793–805.

Chowdhury, S., Sharma, A., 2011. Global sea surface temperature forecasts using a pairwise dynamic combination approach. J. Clim. 24, 1869–1877.

Chumchean, S., Seed, A., Sharma, A., 2006a. Correcting of real-time radar rainfall bias using a kalman filtering approach. J. Hydrol. 317, 123–137.

Chumchean, S., Seed, A., Sharma, A., 2008. An operational approach for classifying storms in real-time radar rainfall estimation. J. Hydrol 363, 1–17.

Chumchean, S., Sharma, A., Seed, A., 2003. Radar rainfall error variance and its impact on radar rainfall calibration. Phys. Chem. Earth, Parts A/B/C 28, 27–39.

Chumchean, S., Sharma, A., Seed, A., 2006b. An integrated approach to error correction for real-time radar-rainfall estimation. J. Atmos. Ocean. Technol. 23, 67–79.

Ciach, G.J., Krajewski, W.F., Villarini, G., 2007. Product-error-driven uncertainty model for probabilistic quantitative precipitation estimation with nexrad data. J. Hydrometeorol. 8, 1325–1347.

Devineni, N., Sankarasubramanian, A., 2010. Improved categorical winter precipitation forecasts through multimodel combinations of coupled gcms. Geophys. Res. Lett. 37.

Elo, C.A., 2012. Correcting and Quantifying Radar Data. Technical Report 2. Norwegian Meteorological Institute, Norway.

Engeland, K., Sultan Abdella, Y., Lepioufle, J.M., 2014. Statistical properties of rain rates in mid Norway as seen by a vertically looking micro rain radar (mrr). In: EGU General Assembly Conference Abstracts.

Fassnacht, S., Kouwen, N., Soulis, E., 2001. Surface temperature adjustments to improve weather radar representation of multi-temporal winter precipitation accumulations. J. Hydrol. 253, 148–168.

Fassnacht, S., Soulis, E., Kouwen, N., 1999. Algorithm application to improve weather radar snowfall estimates for winter hydrologic modelling. Hydrol. Process. 13, 3017–3039.

Førland, E., Allerup, P., Dahlström, B., Elomaa, E., Jónsson, T., Madsen, H., Perälä, J., Rissanen, P., Vedin, H., Vejen, F., 1996. Manual for Operational Correction of Nordic Precipitation Data. Technical Report 24/96. Norwegian Meteorological Institute,DNMI, Oslo, Norway.

Germann, U., Joss, J., 2004. Operational measurement of precipitation in mountainous terrain. In: Weather Radar. Springer, pp. 52–77.

Goudenhoofdt, E., Delobbe, L., 2009. Evaluation of radar-gauge merging methods for quantitative precipitation estimates. Hydrol. Earth Syst. Sci. 13, 195–203.

Haberlandt, U., 2007. Geostatistical interpolation of hourly precipitation from rain gauges and radar for a large-scale extreme rainfall event. J. Hydrol. 332, 144–157.

Hailegeorgis, T.T., Alfredsen, K., Abdella, Y.S., Kolberg, S., 2016. Evaluation of storage–discharge relationships and recession analysis-based distributed hourly runoff simulation in large-scale, mountainous and snow-influenced catchment. Hydrol. Sci. J. 61, 2872–2886.

Hasan, M.M., Sharma, A., Johnson, F., Mariethoz, G., Seed, A., 2016a. Merging radar and in situ rainfall measurements: an assessment of different combination algorithms. Water Resour. Res. 52, 8384–8398.

Hasan, M.M., Sharma, A., Mariethoz, G., Johnson, F., Seed, A., 2016b. Improving radar

rainfall estimation by merging point rainfall measurements within a model combination framework. Adv. Water Resour. 97, 205–218.
Hutchinson, M.F., 1998a. Interpolation of rainfall data with thin plate smoothing splines. part i: two dimensional smoothing of data with short range correlation. J. Geogr. Inf. Decis. Anal. 2, 139–151.
Hutchinson, M.F., 1998b. Interpolation of rainfall data with thin plate smoothing splines. part ii: analysis of topographic dependence. J. Geogr. Inf. Decis. Anal. 2, 152–167.
Hwang, Y., Clark, M., Rajagopalan, B., Leavesley, G., 2012. Spatial interpolation schemes of daily precipitation for hydrologic modeling. Stoch. Environ. Res. Risk Assess. 26, 295–320.
Joss, J., Waldvogel, A., Collier, C., 1990. Precipitation measurement and hydrology. In: Radar in Meteorology: Battan Memorial and 40th Anniversary Radar Meteorology Conference. American Meteorological Society, pp. 577–606.
Khan, M.Z.K., Mehrotra, R., Sharma, A., Sankarasubramanian, A., 2014. Global sea surface temperature forecasts using an improved multimodel approach. J. Clim. 27, 3505–3515.
Killingtveit, Å., 1976. Water Balance Study in Sagelva Research Basin (In Norwegian: En Studie Av Vannbalansen I Sagelva Hydrologiske Forskningsfelt). Ph.D. thesis. Institutt for vassbygging, Norges tekniske hgskole, Trondheim.
Kim, S., Parinussa, R.M., Liu, Y.Y., Johnson, F.M., Sharma, A., 2016. Merging alternate remotely-sensed soil moisture retrievals using a non-static model combination approach. Rem. Sens. 8, 518.
Kirchner, J.W., 2009. Catchments as simple dynamical systems: catchment characterization, rainfall-runoff modeling, and doing hydrology backward. Water Resour. Res. 45.
Koistinen, J., Pohjola, H., 2014. Estimation of ground-level reflectivity factor in operational weather radar networks using vpr-based correction ensembles. J. Appl. Meteorol. Climatol. 53, 2394–2411.
Krajewski, W., Smith, J., 2002. Radar hydrology: rainfall estimation. Adv. Water Resour. 25, 1387–1394.
Krajewski, W.F., 1987. Cokriging radar-rainfall and rain gage data. J. Geophys. Res.: Atmosphere 92, 9571–9580.
Lall, U., Sharma, A., 1996. A nearest neighbor bootstrap for resampling hydrologic time series. Water Resour. Res. 32, 679–693.
Lussana, C., Elo, C.A., Rønning, S.S., 2016a. KliNoGrid RR-Rad. Technical Report 19. Norwegian Meteorological Institute, Norway.
Lussana, C., Ole, E.T., Francesco, U., 2016b. seNorge v2.0: an Observational Gridded Dataset of Temperature for Norway. Technical Report 14. Norwegian Meteorological Institute, Norway.
Marshall, J.S., Palmer, W.M.K., 1948. The distribution of raindrops with size. J. Meteorol. 5, 165–166.
Mehrotra, R., Sharma, Ashish, 2006. A nonparametric stochastic downscaling framework for daily rainfall at multiple locations. Journal of Geophysical Research: Atmospheres 111 (D15) Wiley Online Library.
Nychka, D., Furrer, R., Sain, S., 2017. fields: tools for spatial data. r package version 9.0. http://cran.r-project.org/package=fields, Accessed date: 20 October 2017.
Oke, A., Frost, A., Beesley, C., 2009. The use of trmm satellite data as a predictor in the spatial interpolation of daily precipitation over Australia. In: Proceedings of the 18th World IMACS/MODSIM Congress.
Overeem, A., Holleman, I., Buishand, A., 2009. Derivation of a 10-year radar-based climatology of rainfall. J. Appl. Meteorol. Climatol. 48, 1448–1463.
Rabiei, E., Haberlandt, U., 2015. Applying bias correction for merging rain gauge and radar data. J. Hydrol. 522, 544–557.
Rohrer, M., 1989. Determination of the transition air temperature from snow to rain and intensity of precipitation. In: WMO IASH ETH International Workshop on Precipitation Measurement, pp. 475–582.
Saltikoff, E., Lopez, P., Taskinen, A., Pulkkinen, S., 2015. Comparison of quantitative snowfall estimates from weather radar, rain gauges and a numerical weather prediction model. Boreal Environ. Res. 20, 667–678.
Sharma, A., Mehrotra, R., 2014. An information theoretic alternative to model a natural system using observational information alone. Water Resour. Res. 50, 650–660.
Sharma, A., Mehrotra, R., Li, J., Jha, S., 2016. A programming tool for nonparametric system prediction using partial informational correlation and partial weights. Environ. Model. Softw 83, 271–275.
Silverman, B.W., 1986. Density Estimation for Statistics and Data Analysis, vol. 26 CRC press.
Sinclair, S., Pegram, G., 2005. Combining radar and rain gauge rainfall estimates using conditional merging. Atmos. Sci. Lett. 6, 19–22.
Sivasubramaniam, K., Sharma, A., Alfredsen, K., 2018. Estimating radar precipitation in cold climates: the role of air temperature within a non-parametric framework. Hydrol. Earth Syst. Sci. 22, 6533–6546. https://doi.org/10.5194/hess-22-6533-2018. https://www.hydrol-earth-syst-sci.net/22/6533/2018/.
Smith, M.B., Seo, D.J., Koren, V.I., Reed, S.M., Zhang, Z., Duan, Q., Moreda, F., Cong, S., 2004. The distributed model intercomparison project (dmip): motivation and experiment design. J. Hydrol. 298, 4–26.
Syed, K.H., Goodrich, D.C., Myers, D.E., Sorooshian, S., 2003. Spatial characteristics of thunderstorm rainfall fields and their relation to runoff. J. Hydrol. 271, 1–21.
Tait, A., Henderson, R., Turner, R., Zheng, X., 2006. Thin plate smoothing spline interpolation of daily rainfall for New Zealand using a climatological rainfall surface. Int. J. Climatol. 26, 2097–2115.
Uijlenhoet, R., 2001. Raindrop size distribution and radar reflectivity-rain rate relationships for radar hydrology. Hydrol. Earth Syst. Sci. 5, 615–627.
Villarini, G., Krajewski, W.F., 2010. Review of the different sources of uncertainty in single polarization radar-based estimates of rainfall. Surv. Geophys. 107–129.
Villarini, G., Serinaldi, F., Krajewski, W.F., 2008. Modeling radar-rainfall estimation uncertainties using parametric and non-parametric approaches. Adv. Water Resour. 31, 1674–1686.
Vogl, S., Laux, P., Qiu, W., Mao, G., Kunstmann, H., 2012. Copula-based Assimilation of Radar and Gauge Information to Derive Bias-Corrected Precipitation Fields.
Wasko, C., Sharma, A., Rasmussen, P., 2013. Improved spatial prediction: a combinatorial approach. Water Resour. Res. 49, 3927–3935.
Wilson, J.W., Brandes, E.A., 1979. Radar measurement of rainfall a summary. Bull. Am. Meteorol. Soc. 60, 1048–1058.
Woldemeskel, F.M., Sivakumar, B., Sharma, A., 2013. Merging gauge and satellite rainfall with specification of associated uncertainty across Australia. J. Hydrol. 499, 167–176.
Wolff, M., Isaksen, K., Petersen-Øverleir, A., Ødemark, K., Reitan, T., Brækkan, R., 2015. Derivation of a new continuous adjustment function for correcting wind-induced loss of solid precipitation: results of a Norwegian field study. Hydrol. Earth Syst. Sci. 19, 951–967.